Ca2+ activation of heart mitochondrial oxidative phosphorylation: role of the F0/F1-ATPase

Paul R. Territo, Vamsi K. Mootha, Stephanie A. French and Robert S. Balaban

Am J Physiol Cell Physiol 278:423-435, 2000.

Am. J. Physiol. Cell Physiol.
278: C423–C435, 2000.

Ca^{2+} activation of heart mitochondrial oxidative phosphorylation: role of the F_0/F_1-ATPase

PAUL R. TERRITO, VAMSI K. MOOTHA, STEPHANIE A. FRENCH, AND ROBERT S. BALABAN
Laboratory of Cardiac Energetics, National Heart, Lung, and Blood Institute, National Institutes of Health, Bethesda, Maryland 20892-1061

Territo, Paul R., Vamsi K. Mootha, Stephanie A. French, and Robert S. Balaban. Ca^{2+} activation of heart mitochondrial oxidative phosphorylation: role of the F_0/F_1-ATPase. *Am. J. Physiol. Cell Physiol.* 278: C423–C435, 2000.—Ca^{2+} has been postulated as a cytosolic second messenger in the regulation of cardiac oxidative phosphorylation. This hypothesis draws support from the well-known effects of Ca^{2+} on muscle activity, which is stimulated in parallel with the Ca^{2+}-sensitive dehydrogenases (CaDH). The effects of Ca^{2+} on oxidative phosphorylation were further investigated in isolated porcine heart mitochondria at the level of metabolic driving force (NADH or $\Delta\psi$) and ATP production rates (flow). The resulting force-flow (F-F) relationships permitted the analysis of Ca^{2+} effects on several putative control points within oxidative phosphorylation, simultaneously. The F-F relationships resulting from additions of carbon substrates alone provided a model of pure CaDH activation. Comparing this curve with variable Ca^{2+} concentration ($[Ca^{2+}]$) effects revealed an approximate twofold higher ATP production rate than could be explained by a simple increase in NADH or $\Delta\psi$ via CaDH activation. The half-maximal effect of Ca^{2+} at state 3 was 157 nM and was completely inhibited by ruthenium red (1 μM), indicating matrix dependence of the Ca^{2+} effect. Arsenate was used as a probe to differentiate between F_0/F_1-ATPase and adenylate translocase activity by a futile recycling of ADP-arsenate within the matrix, catalyzed by the F_0/F_1-ATPase. Ca^{2+} increased the ADP arsenylation rate more than twofold, suggesting a direct effect on the F_0/F_1-ATPase. These results suggest that Ca^{2+} activates cardiac aerobic respiration at the level of both the CaDH and F_0/F_1-ATPase. This type of parallel control of both intermediary metabolism and ATP synthesis may provide a mechanism of altering ATP production rates with minimal changes in the high-energy intermediates as observed in vivo.

metabolism; ATP synthesis; dehydrogenase; force-flow analysis

MOST BIOLOGICAL SYSTEMS are capable of maintaining a steady-state metabolism by balancing work with biochemical energy conversion (21, 35, 40). How this metabolic steady state is achieved and controlled in the intact cell is still actively debated. The current study focuses on the regulation and control of mitochondrial energy conversion, a key element in energy metabolism of many tissues.

The mitochondrion, a putative symbiont (10), has been domesticated to perform a primary role in cellular energy metabolism. This organelle produces the major high-energy intermediate in the cytosol, ATP, by oxidative phosphorylation of ADP (4). Indeed, most of the external work performed by the mitochondrion is the production and delivery of ATP to the cytosol. The regulation of mitochondrial ATP production has been suggested to occur by a cytosolic feedback mechanism, relying on ATP hydrolysis with work for ADP and P_i generation (8). Through this mechanism, ATP synthesis was envisioned to follow ATP hydrolysis in the cytosol, paced by ADP concentration ([ADP]) and [P_i]. Studies in the heart (1, 40), brain (20), liver (41), kidney (73), and smooth muscle (72) have demonstrated that the dynamic changes in ADP and P_i with work do not adequately support a simple kinetic feedback model. Most notably are cardiac ATP hydrolysis/synthesis rates, which can change severalfold without a change in cytosolic [ADP] or [P_i] (40). These results suggest that the cytosolic network controlling work and ATP hydrolysis contains elements that modulate mitochondrial ATP production in parallel. This would permit changes in workload with minimal alterations in metabolic intermediates, such as ATP, ADP, or P_i. For this scheme to work in the heart, a cytosolic signaling system must exist that can activate both the contractile activity and oxidative phosphorylation in parallel.

An example of a single cytosolic transducer that could activate both work and biochemical energy conversion in the heart is Ca^{2+} (for reviews see Refs. 29, 33, and 34). Cytosolic [Ca^{2+}] ($[Ca^{2+}]_c$) is important in the activation of cardiac muscle contraction (56, 70). Elevation of $[Ca^{2+}]_c$ results in an electrophoretic uniport (13, 61) and RaM-dependent (28) matrix accumulation of Ca^{2+} (reviewed in Ref. 27). This accumulation enhances substrate conversion via the Ca^{2+}-sensitive dehydrogenases (CaDH), i.e., pyruvate, isocitrate, and 2-oxoglutarate dehydrogenases (32, 49). CaDH activation increases the maximum rate of oxidative phosphorylation by augmenting the delivery of NADH to the respiratory chain, thereby increasing the thermodynamic driving force for ATP synthesis. Augmenting NADH delivery increases the maximum respiratory rate of heart mitochondria in a near linear fashion with concentration (51, 54, 60, 65). In addition, Ca^{2+} has been suggested to modify the ATP synthetic enzyme complex of the mitochondrion, the F_0/F_1-ATPase (62, 77), and the adenine nucleotide translocase in the liver (52, 53). These latter effects suggest that Ca^{2+} may control mitochondrial work (i.e., ATP production) in a pattern similar to cytosolic work (i.e., muscle contraction in the heart) by

stimulating both the supporting intermediary metabolism and work in parallel. This parallel scheme of activation, within the cytosol and mitochondrion, could result in an increased ATP production rate for work with minimal changes in high-energy intermediates, as previously described in intact heart (5, 35, 40, 67).

The purpose of this study was to test the hypothesis that physiological [Ca^{2+}] activates the F_0/F_1-ATPase, in addition to CaDH, resulting in a parallel stimulation of mitochondrial ATP production at both the carbon substrate oxidation and ADP phosphorylation steps. To perform this task, the effects of [Ca^{2+}] on isolated porcine heart mitochondria were studied while simultaneously monitoring oxygen consumption [mitochondrial $\dot{V}O_2$ ($m\dot{V}O_2$)] and the metabolic driving forces at NADH and mitochondrial membrane potential ($\Delta\psi$). These studies permitted the separation of net effects of CaDH activation and F_0/F_1-ATPase activity in the intact mitochondrion.

MATERIALS AND METHODS

Heart isolation and perfusion. Porcine hearts were harvested from heparinized (250 IU/kg iv) stage III (plane 4) α-chloralose anesthetized animals (100 mg/kg iv) through a midline thoracotomy. All procedures performed were in accordance with the guidelines listed in the Animal Care and Welfare Act (7 U.S.C. 2142 § 13). The isolated heart was quickly perfused retrogradely via the aorta with 500 ml (4°C) *buffer A* (280 mM sucrose, 10 mM HEPES, and 0.2 mM EDTA at pH 7.2) to facilitate removal of blood and extracellular Ca^{2+}. The perfused heart was cleared of all epicardial fat, blood vessels, atria, and right ventricular myocardium. The left ventricular myocardium was weighed and quartered for use in mitochondrial isolation.

Mitochondrial isolation and fluorescence standard loading. Mitochondria were isolated according to methods described in Ref. 25. Briefly, four 25-g sections of left ventricle were finely minced using scissors in 50 ml of *buffer A*. The minced ventricle was then treated for 15 min with 0.5 mg bovine pancreas trypsin per gram of tissue (Sigma, St. Louis, MO). The supernatant was then poured off and replaced with *buffer A* containing 1 mg/ml BSA and trypsin inhibitor (2.6 mg/g tissue), and maintained at 4°C for 5 min. On completion, the supernatant was replaced with *buffer A* containing 1 mg/ml BSA, and the suspension was quickly homogenized with two grades of Teflon homogenizers (Thomas Scientific, Swedesboro, NJ). This homogenate was centrifuged in 60-ml aliquots for 10 min (600 *g*) and the pellets discarded. The supernatant was recentrifuged and washed with *buffer A* (containing 1 mg/ml BSA) at 8,000 *g* for 15 min. The pelleted mitochondria were resuspended in 4 ml of *buffer B* (137 mM KCl, 10 mM HEPES, 2 mM P_i, 2.5 mM $MgCl_2$, 0.5 mM EDTA, pH 7.2) and stored on ice. Of the 4 ml of isolated mitochondria, 3.5 ml were loaded at 1 nmol/nmol cytochrome A (for assay see below) with 5-(6)-carboxy-2′-7′-dichlorofluoresceindiacetate succinimidyl ester (CF; Molecular Probes, Eugene, OR) at 4°C for 10 min for light-scattering corrections (14). Loaded and unloaded mitochondria were washed and repelleted (8,000 *g* for 10 min) three times (twice in *buffer A* containing 1 mg/ml BSA and once in plain *buffer A*) to remove any unloaded CF. The third mitochondrial pellet was resuspended in plain *buffer B* at ~15 nmol cytochrome A/ml and kept on ice until use.

Mitochondrial cytochrome A assay. Mitochondrial cytochrome A content was determined spectrophotometrically as previously described (2). Briefly, mitochondria were solubilized with a 2% solution of Triton X-100 in 100 mM Na_3PO_4 buffer (pH 7), and difference spectra were obtained with a spectrophotometer (Lambda 3B; Perkin-Elmer) between oxidized and hydrosulfide reduced mitochondrial solutions. The cytochrome content was determined as described previously (2) using the 605-nm, 630-nm wavelength pair, and a molar extinction coefficient of 12 mM^{-1}.

Respiratory rate ($m\dot{V}O_2$), membrane potential ($\Delta\psi$), and NADH fluorescence. To determine the effects of Ca^{2+} on metabolism, it was necessary to deplete heart mitochondria of endogenous Ca^{2+}. This was achieved with 6 min of incubation in *buffer C* (125 mM KCl, 20 mM HEPES, 15 mM NaCl, 5 mM $MgCl_2$, 1 mM K_2EDTA, 1 mM EGTA, 2 mM P_i, 0.1 mM malate, and 4 μM TPP^+, with 3.4 mM Na_2ATP added fresh daily, pH 7) in the absence of extraneous carbon substrates. Postincubation, substrates and Ca^{2+} were added to the mitochondrial suspension to establish new steady states. Free [Ca^{2+}] in *buffer C* was determined from binding affinity constants previously reported (23). In all cases except where noted, [Ca^{2+}] are presented as calculated free concentrations.

The rate of mitochondrial O_2 consumption ($m\dot{V}O_2$) was determined in a modified closed-system respirometer described previously (51) and was used to estimate steady-state ATP production rate. Briefly, the ADP-P_i-driven rate of O_2 consumption (state 3) and subsequent state 4 rate were monitored in a custom-thermostatted chamber (37°C) with a polarographic oxygen electrode calibrated to room air. State 3 was defined as steady-state maximal ADP-P_i-driven respiration in substrate-energized mitochondria, whereas state 4 was respiration in the absence of ADP-P_i (8). Experiments were performed at mitochondrial concentrations of 1 nmol cytochrome A/ml. A magnetic stirring bar provided mixing of the mitochondrial suspension.

Oxygen consumption has the units of nanomoles of oxygen per nanomole of cytochrome A per minute and was calculated as follows

$$m\dot{V}O_2 = \left(\frac{b_O \cdot 60 \cdot \alpha \cdot V_c}{100 \cdot Cyt_a}\right) \quad (1)$$

where b_O is the calculated slope from digitized oxygen recordings in change in percentage of oxygen per second, α is the solubility of oxygen in buffer for a given salt content in nanomoles per milliliter, V_c is the volume of the chamber in milliliters, and cytochrome A is the cytochrome A content in nanomoles. The oxygen solubility used was 199 nmol/ml at 37°C (9). The ATP production rate was estimated to be 2.8 moles ATP per mole of oxygen (O) consumed (see ADP/O calculations below). Estimates of mitochondrial integrity were determined from the respiratory control ratios (RCR) of $m\dot{V}O_2$ at state 3 and state 4 in *buffer B*, which contained 5 mM glutamate, 5 mM malate, 2 mM P_i, and 4 μM TPP^+, and were stimulated with a single addition of 1.3 mM ADP (final). Where applicable, glutamate (G) and malate (M) were added in equimolar proportions, where 5 mM G/M represents the concentration of each substrate in the mixture.

The redox state of pyridine dinucleotides was monitored concurrently using a commercial spectroflurometer (LS50B; Perkin-Elmer) connected via an external fiber-optic bundle that was coupled to an embedded sapphire window in the experimental chamber. The entire respirometry system was housed in a light-tight box to minimize extraneous light. Mitochondrial fluorescence spectra were collected using an excitation of 340 nm (10-nm slit, 350-nm cutoff filter) and emission of 360–660 nm at 1,500 nm/s with a 15-nm slit. Control spectra were obtained in fully oxidized (0.067 mM

ADP) and reduced (5 mM G/M) mitochondria, both with and without CF. From these difference spectra, model spectra of NADH (M_{NADH}) and CF (M_{CF}) were constructed. Additionally, spectra were obtained from G-10 sephadex beads (size 40–120 μm) at 1 mg/ml suspended in *buffer B* to model excitation light bleedthrough (M_{EBT}). Model spectra (M_{NADH}, M_{CF}, and M_{EBT}) were then fitted with a multiple linear regression and compared against experimental spectra to eliminate both primary and secondary inner filter effects as previously described (25). The linear fit was described by the following relationships

$$F = F_{NADH} + F_{CF} + F_{EBT} \quad (2)$$

$$F_{NADH} = I_{NADH} \cdot M_{NADH} \quad (2.1)$$

$$F_{CF} = I_{CF} \cdot M_{CF} \quad (2.2)$$

$$F_{EBT} = I_{EBT} \cdot M_{EBT} \quad (2.3)$$

where F is the combined fit for all model (M) components and F_{NADH}, F_{CF}, and F_{EBT} refer to the corresponding fits for NADH, CF, and EBT, respectively. The algorithm determined the coefficients I_{NADH}, I_{CF}, and I_{EBT} as estimates of each peak's contribution to the total fluorescence spectrum. All regressions were performed iteratively until the sum of squares convergence was achieved using the Marquardt-Levenberg algorithm written in Interactive Data Language (version 5.1, Research Systems). The algorithm produces *1*) the coefficients of the model spectra, *2*) SD for the coefficients, *3*) an *F* test for fit between model and experimental data, and *4*) multiple linear correlation coefficients for the fitted spectra. In all cases, model and experimental spectra had a high degree of concordance (0.99 ± 0.0001, n = 1,340). Data for each experimental spectrum was presented as I_{NADH}/I_{CF} ratios to correct for inner filter effects, and normalized within each preparation to mitochondria with 5 mM G/M + 535 nM free [Ca^{2+}] at state 3.

Mitochondrial membrane potential (Δψ) was determined from the Nernst equilibrium of 4 μM TPP^+ across the mitochondrial membrane. This lipophilic cation was detected using a TPP^+ ion-selective electrode (model MEH2SW20; World Precision Instruments) and an Ag-AgCl reference electrode (model MI 402; Microelectrodes). Both electrodes were connected to a high-impedance pH meter (model 901; Orion Research) and the output amplified. The resulting signal was digitally sampled at 2 Hz via an analog-to-digital (A/D) converter and recorded using a custom program written in Workbench-Mac (Strawberry Tree). The correlation between absolute [TPP^+] and electrode voltages was determined daily using an automated micropipetter (Microlab 500; Hamilton) to establish standard curves. It was determined that the electrode drifted over time; however, this drift could be accounted for by changes in the intercept of the standard curve over time and did not significantly alter the slope. Nonspecific binding of TPP^+ to mitochondrial membranes was corrected for according to the methods previously described (59). Drift- and binding-corrected membrane potential were calculated according to the following equation

$$\Delta\psi = \frac{2.303\,RT}{ZF} \cdot \log_{10}\left\{\frac{(V_m + K)\,[Y_o + m_o e^{m_1(E_v - \Delta E_d)}]}{V_t[TPP^+]_T - (V_c - \frac{K}{R_c})\,[Y_o + m_o e^{m_1(E_v - \Delta E_d)}]}\right\} \quad (3)$$

where RT/F is the Nernst factor (R is gas constant, T is temperature, and F is the Faraday constant), Z is the valence of TPP^+, V_m is the volume of the mitochondria (in microliters), V_t is the total volume of the system (in microliters), V_c is the volume of the experimental chamber (in microliters), $[TPP^+]_T$ is the total concentration of TPP^+ in the experimental buffer (in micromolar), K is the nonspecific binding constant for TPP^+ (6 μl/nmol cytochrome A), R_c is the partition coefficient for nonspecific binding, E_v is the millivolt reading from the electrode, ΔE_d is the electrode drift in millivolts (empirically determined before each run), and Y_o, m_o, and m_1 are the coefficients describing the standard curve using a three-parameter exponential growth regression (Sigma Plot version 4.0; SPSS). Although mitochondrial volume has been shown to change with ATP production rate and [Ca^{2+}] (25), volume estimates in these preparations varied by only 5.9 ± 0.7% (n = 12), which equated to <1% error in estimating Δψ over the entire range of substrate and Ca^{2+} concentrations used. The sensitivity of the TPP^+ electrode to [Ca^{2+}] was evaluated over the entire range of [Ca^{2+}] used in these studies. With the extramitochondrial [TPP^+] of 4 μM, no dependence of [Ca^{2+}] was found using this ion-selective electrode system (data not shown).

ADP-to-oxygen ratio. ADP-to-oxygen ratios (ADP/O) were calculated according to methods previously described (8, 36). Briefly, the oxygen consumed from the single addition of ADP (500 μM final concentration) was determined from the amount of oxygen consumed per mole of ADP added to mitochondria in *buffer C*. Analysis was performed using a custom program written in IDL.

Luminometric ATP determination. In an effort to validate the ADP/O ratio as a reliable estimate of ATP production rate and to evaluate the possibility that [Ca^{2+}] used in this study significantly uncoupled oxidative phosphorylation, luciferin/luciferase luminescent assays of ATP production were performed in the presence and absence of Ca^{2+} at state 3. Mitochondria were incubated in *buffer C* (minus ATP) containing 40 μg/ml luciferase and 715 μM D-luciferin for 6 min. Postincubation, mitochondria were reduced with 5 mM G/M, and maximal state 3 respiration was initiated with a 1.3 mM bolus of ADP (final concentration). At the end of each experiment, a known standard of ATP (160 μM) was added to the reaction mixture serving as an internal control for interexperimental variation. Total photons were collected with a custom-built photomultiplier tube assembly optically coupled to the thermostatted 37°C reaction chamber via a liquid light guide. Simultaneous measures of oxygen consumption were collected using a polarographic oxygen electrode (see above). Voltages were digitally sampled at 10 Hz with a 12-bit A/D converter and recorded using a tailor-made program written in Workbench-Mac.

Determination of absolute [ATP] above 200 μM is difficult with this approach due to the nonlinear photon emission rates caused by product inhibition (i.e., oxyluciferin) and loss of quantum yield (18, 19, 44, 45). To maintain constant state 3 respiratory rates where substrates are not limiting, the [ADP] and, subsequently, synthesized [ATP] were used at concentrations >200 μM (51). It was reasoned that if the ATP production rate was held constant by appropriate dilution of the mitochondrial concentration in the presence of Ca^{2+}, the time intensity curves of the control and Ca^{2+}-stimulated conditions could be directly compared, thus minimizing the kinetic complications of the luciferin/luciferase assay. The rate of ATP production was assumed to be proportional to the $m\dot{V}O_2$ under both conditions, with no coupling loss caused by Ca^{2+} at 535 nM. Ca^{2+}-stimulated mitochondria were diluted relative to controls (Ca^{2+}-depleted) by the following equation

$$[Cyt_a]_{dil} = \frac{(m\dot{V}O)_{Ca^{2+}}}{(m\dot{V}O_2)_0} \quad (4)$$

where $[Cyt_a]_{dil}$ is the cytochrome A dilution factor for Ca^{2+}-stimulated respiration $[(m\dot{V}O_2)_{Ca^{2+}}]$ to achieved identical respiratory rates when compared with controls$[(m\dot{V}O_2)_0]$. This dilution resulted in identical absolute oxygen consumption rates in the chamber with both control and Ca^{2+}-stimulated mitochondria. Provided that $m\dot{V}O_2$ was associated with the same ATP/O ratio with and without Ca^{2+} stimulation, the luciferin/luciferase photon emission time courses should be identical for both conditions.

Statistical analysis. Slope determinations between treatment groups were calculated by a first-order least-squares linear regression (Statistica version 5.0; Statsoft). This analysis determines *1*) the regression coefficient, *2*) the equation of the line describing the relationship, and *3*) the probability that the slope of the line is significantly different from zero. Individual slopes (between $m\dot{V}O_2$ and NADH, or $\Delta\psi$), ADP/O ratios, ATP production, and carbonyl cyanide *p*-(trifluoromethoxy)phenylhydrazone (FCCP) dose-response curves at each level were then compared using a single-factor-dependent variable *t*-test (Statistica version 5.0). Where appropriate, values are means ± 1 SE. In all cases, the fiduciary level of significance was taken at $P \leq 0.05$.

RESULTS

Mitochondrial characterization. Isolated mitochondria in this preparation produced a high yield of tightly coupled mitochondria with an average yield of 0.9 ± 0.06 nmol cytochrome A/g wet wt myocardium ($n = 29$), corresponding to 2.5% of the total cytochrome A in pig heart (51). Estimates of mitochondrial integrity were determined by the RCR and were performed in *buffer B* with 5 mM G/M, 2 mM P_i, 4 μM TPP^+, and a single addition of 1.3 mM ADP (final concentration) (37°C), which allowed for comparison with previous work. The average RCR was 10.5 ± 0.3 ($n = 29$) and ranged between 8 and 14. Mitochondria with RCR of <8 were not used in these studies.

Effects of Ca^{2+} depletion. To determine the physiological affects of Ca^{2+} on mitochondrial energetics, it was necessary to deplete the organelle of endogenous Ca^{2+} and substrates to minimize interexperimental variability. In all cases, mitochondria were Ca^{2+} and substrate depleted with a 6-min incubation in *buffer C* (state 1) (8), which resulted in a significant reduction in $\Delta\psi$ from −143 ± 3 to −121 ± 3 mV ($P \leq 0.05$, $n = 29$). This condition is defined as Ca^{2+} depleted with nominally zero $[Ca^{2+}]$, because some residual Ca^{2+} is likely to present in the system. Addition of substrates (G/M or succinate) and exogenous Ca^{2+} resulted in a repolarization of the mitochondrial membrane to preincubation levels. In studies where minimal CaDH effects were desired, succinate was used as the oxidizable carbon source. Dosing studies with succinate without Ca^{2+} revealed Michaelis-Menten kinetics for state 3 respiratory rates in *buffer C*, with an apparent K_m value 2.46 mM. Maximum ADP-stimulated respiratory rates were attained with 15 mM succinate.

Ca^{2+} optimization. Steady-state kinetics at state 3 and state 4 for Ca^{2+} were determined for NADH driving force and $m\dot{V}O_2$. In Ca^{2+}-depleted mitochondria, state 3 $m\dot{V}O_2$ and NADH increased with $[Ca^{2+}]$ over the range of 1.54 to 1,810 nM (Fig. 1). The kinetics showed saturation with a half-maximal activation ($K_{0.5}$) at 157 nM free $[Ca^{2+}]$ while oxidizing G/M as the substrate. The equations and regression statistics describing these trends are presented in Table 1. The increase in NADH is consistent with the known increase in CaDH activity with Ca^{2+}. The increase in $m\dot{V}O_2$ could be due to increased driving force for ATP production, via in-

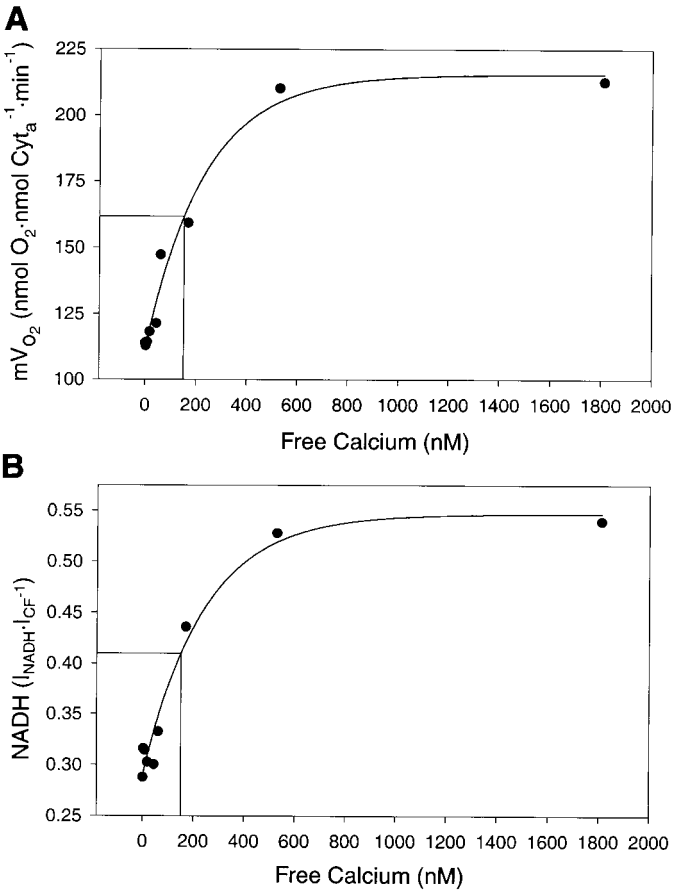

Fig. 1. Ca^{2+} dose-response curves at state 3 respiration. *A*: data are plotted as state 3 mitochondrial $\dot{V}O_2$ ($m\dot{V}O_2$) vs. $[Ca^{2+}]$. *B*: plot of state 3 NADH vs. $[Ca^{2+}]$. Statistical analysis and regression coefficients are presented in Table 1. In all cases, mitochondria were Ca^{2+} depleted as described in MATERIALS AND METHODS, and experiments were performed with 5 mM G/M (glutamate/malate) as the oxidizable carbon source. Cyt_a, cytochrome A; I_{NADH}, NADH coefficient; I_{CF}, 5-(6)-carboxy-2′-7′-dichlorofluoresceindiacetate succinimidyl ester coefficient.

Table 1. *Regression analysis of state 3 condition with $[Ca^{2+}]$*

Measurement	Y_o	a	b	r^2	$K_{0.5}$, nM	n
$m\dot{V}O_2$	111.2	104.5	0.0043	0.98	157.1	9
NADH	0.289	0.258	0.0042	0.97	157.6	9

Relationships for mitochondrial oxygen consumption ($m\dot{V}O_2$) and NADH with $[Ca^{2+}]$ are expressed as $Y = Y_o + a(1 - e^{-bx})$, where Y is oxygen consumption (nmol O_2·nmol Cyt_a^{-1}·min^{-1}) or NADH (I_{NADH}/I_{CF}). Y_o, a, b, r^2, $K_{0.5}$, and n are DC offset, intercept, slope, regression coefficient, half saturation coefficient, and sample size compared with a zero slope, respectively. In all cases, $K_{0.5}$ were calculated by mathematical inversion of the above equation and used the oxygen consumption or NADH values at 1,810 nM $[Ca^{2+}]$. $P \leq 0.0001$, compared with a zero slope.

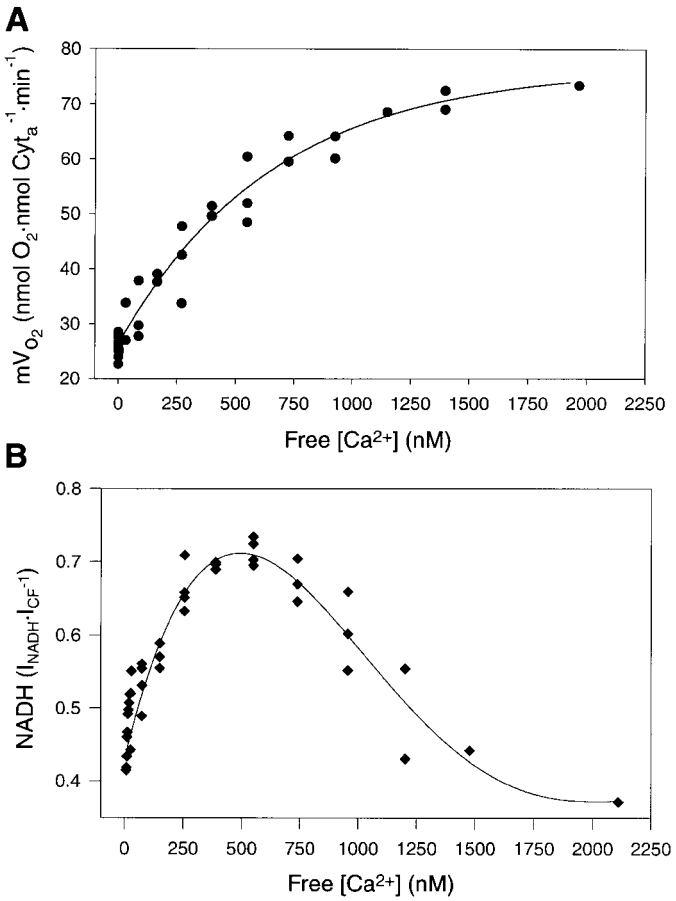

Fig. 2. Ca^{2+} dose-response curves at state 4 respiration. *A*: data are plotted as state 4 $m\dot{V}O_2$ vs. [Ca^{2+}]. *B*: plot of state 4 NADH vs. [Ca^{2+}]. Statistical analysis and regression coefficients for $m\dot{V}O_2$ are presented in Table 2. Due to nonsaturating kinetics, statistical analyses for NADH were not performed. In all cases, mitochondria were Ca^{2+} depleted as described in MATERIALS AND METHODS, and experiments were performed with G/M as the oxidizable carbon source.

creases in NADH, and/or mitochondrial uncoupling by Ca^{2+} transport.

To further evaluate the possibility of Ca^{2+}-dependent uncoupling and select a useful [Ca^{2+}] for this study, $m\dot{V}O_2$ and NADH production rates were evaluated at state 4 where the effects should be amplified. Like state 3, $m\dot{V}O_2$ showed saturation kinetics with [Ca^{2+}] studied (Fig. 2*A*); however, the $K_{0.5}$ was 376.1 nM, which is more than double that seen at state 3 (Table 2). NADH in mitochondria oxidizing G/M at state 4 increased with [Ca^{2+}] <600 nM, whereas at higher concentrations NADH decreased. The calculated optima for NADH levels occurred at 535 nM [Ca^{2+}] (Fig. 2*B*). The decrease in NADH above 600 nM [Ca^{2+}] suggests that significant mitochondrial uncoupling might be occurring above this concentration, dissipating the driving force for ATP synthesis. However, it is unclear to what extent this contributes to the total $m\dot{V}O_2$ observed. Based on the combined state 3 and 4 data, 535 nM was used as the optimal [Ca^{2+}], with minimal deleterious effects.

Table 2. *Regression analysis of state 4 oxygen consumption with [Ca^{2+}]*

Measurement	Y_o	a	b	r^2	$K_{0.5}$, nM	n
$m\dot{V}O_2$	26.3	50.5	0.0015	0.97	376.1	38

Relationship for state 4 oxygen consumption with [Ca^{2+}] is expressed as $Y = Y_o + a(1 - e^{-bx})$, where Y is oxygen consumption (nmol O_2·nmol Cyt_a^{-1}·min^{-1}). Y_o, a, b, r^2, $K_{0.5}$, and n are DC offset, intercept, slope, regression coefficient, half saturation coefficient, and sample size compared with a zero slope, respectively. In all cases $K_{0.5}$ were calculated by mathematical inversion of the above equation and used the oxygen consumption at 1810 nM [Ca^{2+}]. $P \leq 0.0001$, compared with a zero slope.

ADP/O values were determined as a function of [Ca^{2+}] to further evaluate the possibility of Ca^{2+} uncoupling (for data, see Table 4). The ADP/O ratio was constant up to 535 nM [Ca^{2+}], suggesting that any uncoupling caused by Ca^{2+}-dependent transport was not significant at state 3 ATP production rates.

To confirm this indirect measurement, the production of ATP was monitored directly using the luciferin/luciferase assay in intact mitochondria. For this assay, the concentration of mitochondria stimulated by [Ca^{2+}] was reduced relative to control, using *Eq. 4*. Under these conditions, if the ATP/O ratio was constant under Ca^{2+}-depleted and Ca^{2+}-stimulated conditions, the time course of the photon emission should be identical. The magnitude and time courses of the photon emission are presented in Fig. 3*A*. ATP production rate with 535 nM Ca^{2+} was identical for the two conditions ($P > 0.05$, $n = 4$) despite a 1.8-fold lower mitochondrial content. The observation that state 3 $m\dot{V}O_2$ accurately predicted the proper dilution of the mitochondria to match the ATP production rates also suggests that the ATP/O ratio was identical in the presence and absence of Ca^{2+}. These data combined, the ADP/O and ATP production kinetics in the presence and absence of Ca^{2+} demonstrate that Ca^{2+} was not significantly uncoupling respiration at 535 nM.

Dose response to uncoupler. In an effort to evaluate maximally stimulated rates, independent of F_0/F_1-ATPase and adenylate transport (ANT), state 4 Ca^{2+}-depleted mitochondria oxidizing succinate (30 mM) + 535 nM Ca^{2+} were titrated with FCCP in *buffer C*. The results of these studies are shown in Fig. 3*B*. The optimum concentration of FCCP was 33 nM FCCP. Some variation in the optimal concentration of FCCP was found in the absence of Ca^{2+}, with the apparent optimal concentration of FCCP increasing to 50 nM with nominally zero [Ca^{2+}] present.

Ca^{2+} activation of oxidative phosphorylation. The initial study attempted to establish the effect of CaDH activation alone on mitochondrial ATP production. Because Ca^{2+} stimulates CaDH activity, which augments ATP production rate via increasing [NADH] (32, 49), these effects could be simulated by titrating carbon substrates oxidized by CaDH. Using this approach, the relationship between the driving force ([NADH] and/or $\Delta\psi$) and flow ($m\dot{V}O_2 \cong$ ATP synthesis rate as estimated by ADP/O and confirmed by luminometry) would provide a standard curve for [NADH] and $\Delta\psi$-dependent CaDH effects. These force-flow (F-F) relationships are presented in Fig. 4 as the NADH levels or $\Delta\psi$ vs. maximal state 3 rate, with G/M as the CaDH oxidizable

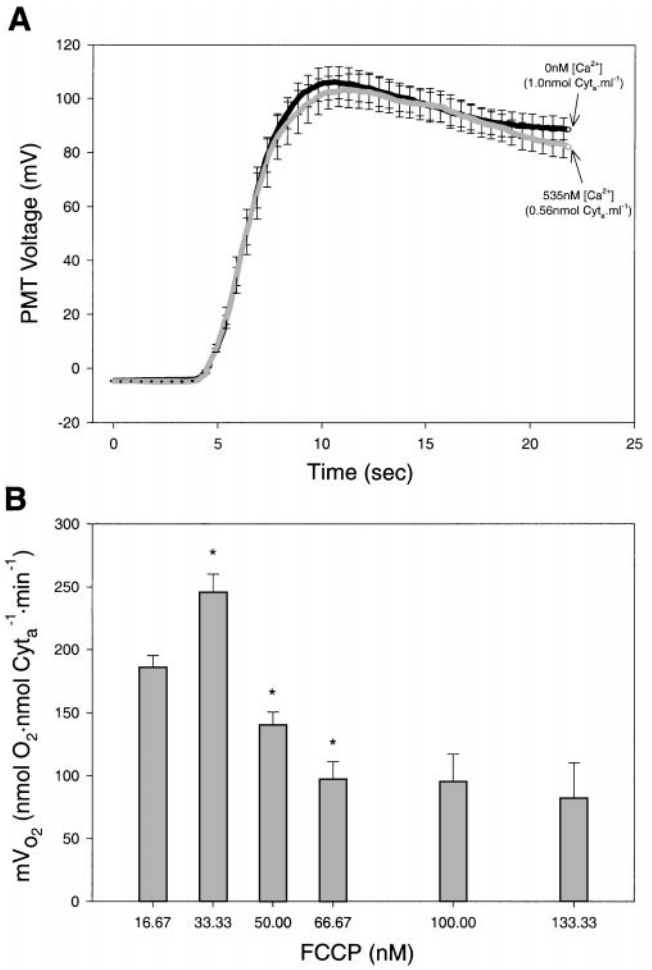

Fig. 3. Mitochondrial ATP production and uncoupling optimization. *A*: luminometric analysis of photon production (≅ATP) in Ca^{2+}-depleted mitochondria oxidizing 5 mM G/M. State 3 respiration was initiated with 1.3 mM bolus of ADP in presence (535 nM) and absence of Ca^{2+}. Metabolic rates from paired experiments were matched in all cases using *Eq. 4*. Data are means ± SE, where SE data are presented at every 50th data point for clarity. *B*: plot of uncoupled respiration ($m\dot{V}O_2$) vs. titration of metabolic uncoupler carbonyl cyanide *p*-(trifluoromethoxy)phenylhydrazone (FCCP; in nM). In all cases, mitochondria were incubated at 37°C for 6 min without substrates, as described in MATERIALS AND METHODS. Data are means ± SE; *significant differences from proceeding condition ($P \leq 0.05$). PMT, photomultiplier tube.

substrates and succinate as the substrate with minimal CaDH contributions in its oxidation pathway. As illustrated by Fig. 4, linear F-F relationships were obtained for NADH and Δψ with $m\dot{V}O_2$ and were in agreement with previous studies (43, 51). Regression statistics and F-F slopes for mitochondria oxidizing G/M and succinate are presented in Table 3. Because the above F-F functions establish the benchmark for the CaDH/NADH response, any deviation from these F-F curves for NADH or Δψ with $[Ca^{2+}]$ would suggest a mechanism other than simple CaDH activation.

The effects of increasing $[Ca^{2+}]$ on state 3 respiration with a fixed level of carbon substrate are also shown in Fig. 4 for comparison. Both G/M and succinate with nominal $[Ca^{2+}]$ failed to support higher $m\dot{V}O_2$ compared with CaDH controls at the same [NADH], indicating

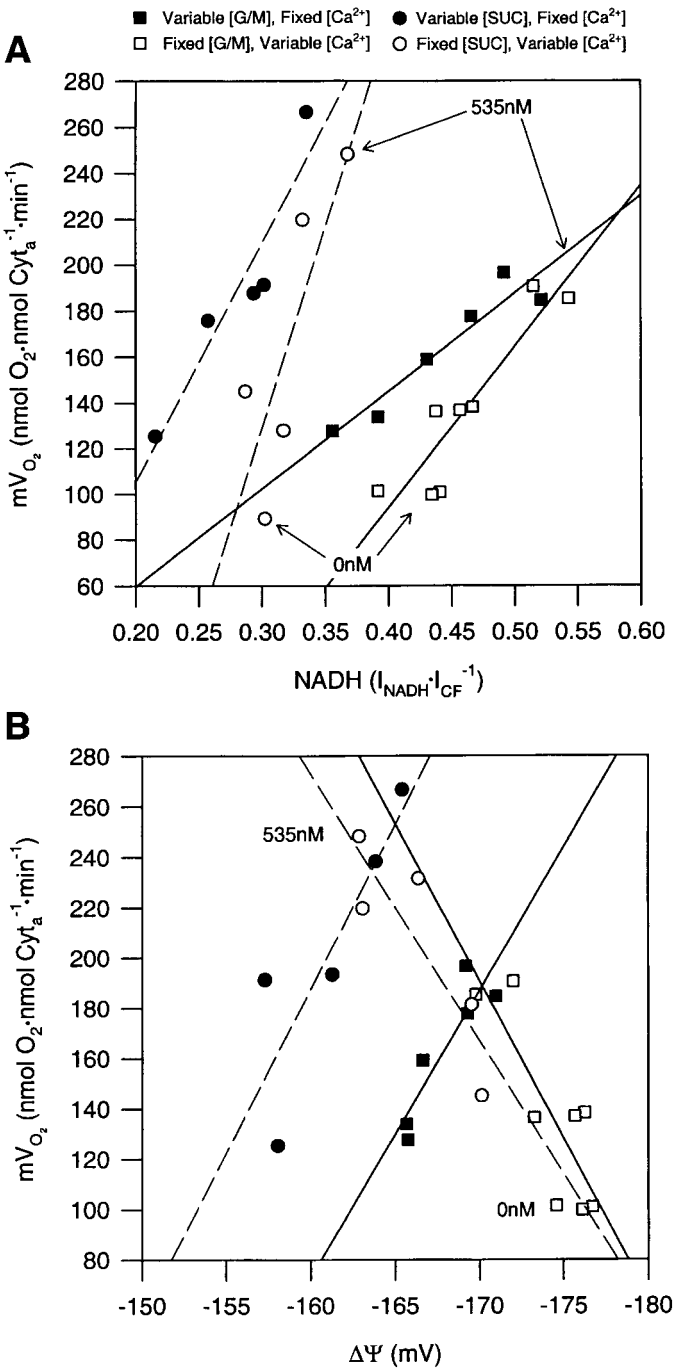

Fig. 4. Representative force-flow (F-F) relationships at state 3 respiration with variable Ca^{2+} and substrates. *A*: data are plotted as $m\dot{V}O_2$ vs. NADH for G/M (squares) and succinate (SUC; circles). Filled symbols represent fixed $[Ca^{2+}]$ with variable [substrate] (control), whereas open symbols are variable $[Ca^{2+}]$ with fixed [substrate]. *B*: plot of $m\dot{V}O_2$ vs. Δψ with either G/M or SUC. Symbols and conditions are as stated in *A*. Solid (G/M) and dashed (SUC) lines are linear regressions, with statistical summary presented in Table 3. Substrate concentrations ranged from 5 to 0.5 mM with G/M and 15 to 1.67 mM with SUC, whereas Ca^{2+} used in these studies was fixed at 535 nM free for control conditions. Under experimental conditions $[Ca^{2+}]$ ranged from 535 to 0 nM free, whereas substrate concentrations were fixed at 5 and 15 mM for G/M and SUC, respectively. In all cases, mitochondria were incubated at 37°C for 6 min, as described in MATERIALS AND METHODS, for Ca^{2+} depletion before commencement of experiments.

Table 3. *Mean force-flow slopes and regression statistics with substrate and Ca^{2+} titration*

Condition	NADH F-F Slope, nmol O_2·nmol Cyt_a^{-1}·min^{-1}·$NADH^{-1}$	r^2	ΔΨ F-F Slope, nmol O_2·nmol Cyt_a^{-1}·min^{-1}·$\Delta\Psi^{-1}$	r^2
Variable [G/M]	286.4 ± 44.4	0.93 ± 0.03	−3.81 ± 0.735	0.87 ± 0.05
Fixed [Ca^{2+}]	(10)		(8)	
Fixed [G/M]	755.3 ± 162.7*	0.92 ± 0.02	10.4 ± 2.94*	0.93 ± 0.03
Variable [Ca^{2+}]	(10)		(8)	
Variable [SUC]	920.0 ± 161.8	0.91 ± 0.04	−10.5 ± 3.66	0.94 ± 0.02
Fixed [Ca^{2+}]	(7)		(10)	
Fixed [SUC]	1561.8 ± 252.4*	0.92 ± 0.04	13.8 ± 4.42*	0.94 ± 0.01
Variable [Ca^{2+}]	(7)		(10)	
Variable [SUC]†			−16.09 ± 2.54	0.95 ± 0.01
Fixed [Ca^{2+}]			(3)	
Fixed [SUC]†			11.54 ± 3.70*	0.95 ± 0.02
Variable [Ca^{2+}]†			(3)	
Variable [G/M]	321.5 ± 71.8	0.87 ± 0.04	−7.38 ± 1.21	0.86 ± 0.05
Fixed [Ca^{2+}]	(6)		(6)	
Variable [G/M]	147.8 ± 71.6*	0.96 ± 0.02	−1.90 ± 0.754*	0.90 ± 0.02
Zero [Ca^{2+}]	(6)		(6)	
Variable [SUC]‡	707.4 ± 140.0	0.96 ± 0.01	−9.73 ± 4.40	0.97 ± 0.02
Fixed [Ca^{2+}]‡	(4)		(4)	
Fixed [SUC]‡	323.6 ± 30.0*	0.91 ± 0.03	3.23 ± 0.792*	0.92 ± 0.04
Variable [Ca^{2+}]‡	(4)		(4)	

Values are means ± SE. [Ca^{2+}] and glutamate/malate ([G/M]) used for each condition are presented in Fig. 4 legend. Succinate (SUC) used in these studies was 3.4, 8.4, and 15 mM. Numbers in parentheses are number of observations and r^2 is combined regression coefficient relative to a slope of zero. *Differences between paired treatment groups ($P \leq 0.05$; dependent variable *t*-test). †Mitochondria oxidizing SUC + 5.8 μM rotenone. Due to the inhibition of site 1 by rotenone, NADH F-F slopes were not possible. ‡Data from mitochondria oxidizing SUC, in the presence of 8.34 μM atractyloside, 200 mM ADP, and 2 mM AsO_4 in the absence of exogenous P_i. $P \leq 0.001$, relative to a slope of zero.

that some step beyond the generation of NADH was inhibiting mVO_2 and/or ATP production at low [Ca^{2+}]. NADH levels increased proportionately with [Ca^{2+}], consistent with the activation of CaDH with G/M, and to a lesser extent with succinate. However, the NADH F-F slopes more than doubled with Ca^{2+} for G/M and succinate (Fig. 4*A* and Table 3), indicating a disproportionate increase in mVO_2 for a given [NADH]. Ruthenium red (1 μM), a Ca^{2+} uniport inhibitor, completely blocked the Ca^{2+} effects, suggesting that matrix [Ca^{2+}] is necessary for activation (data not shown). The significant increases in the NADH F-F slopes with Ca^{2+} indicated that mVO_2 increased more than could be predicted by a simple increase in NADH through CaDH activation. Moreover, these data also show that, at the same NADH driving force, respiration is augmented severalfold with the addition of Ca^{2+}.

These findings were further confirmed by similar experiments in mitochondria titrated with G/M in the presence (535 nM) and absence (nominally zero) of [Ca^{2+}] (Fig. 5). In both cases, mitochondria exhibit a linear dependence with [G/M]; however, the NADH F-F slope more than doubled with the addition of optimal Ca^{2+} (Table 3). As with previous experiments, mVO_2 was inhibited in the absence of significant [Ca^{2+}], despite adequate NADH driving force and identical [G/M].

Both of these studies with constant or variable [G/M] demonstrated an increase in NADH with Ca^{2+} consistent with CaDH activation described previously (42, 51). However, the degree of NADH increase with Ca^{2+} was not adequate to explain the increases in state 3 ATP synthesis rate observed, suggesting a mechanism in addition to CaDH.

More revealing was the Δψ data, where, instead of Δψ increasing with [Ca^{2+}] as occurred with CaDH controls, Δψ decreased, resulting in a change in sign and reversal of the Δψ F-F slope (Fig. 4*B*; Table 3). Similar results were obtained with succinate in the presence of 5.8 μM rotenone (Table 3), an inhibitor of site 1, thus eliminating NADH contributions completely. The fact that the Δψ F-F slopes were identical, within statistical limits, in the presence and absence of rotenone indicates that the activation by Ca^{2+} is downstream of site 1. Clearly, the major driving force for ANT and ATP synthesis decreased with Ca^{2+}, the opposite of what would be predicted from a simple increase in CaDH activity. Provided these interpretations are correct, titrating substrates (G/M) with and without Ca^{2+} should result in a similar F-F slope direction; however, the absolute magnitude should be considerably lower without Ca^{2+}. The results of these experiments are presented in Fig. 5*B* and Table 3, confirming these predictions. The drop in Δψ (less negative) observed with increasing ATP production suggests that ATP synthesis (F_0/F_1-ATPase) and ANT have increased in the presence of Ca^{2+}, despite significantly lower driving forces. These increases occurred without a decrease in the ADP/O ratio with increasing [Ca^{2+}], thus providing no evidence for significant uncoupling via inner membrane recycling of Ca^{2+} (Table 4). Luminometric estimates of ATP synthesis rates further support this contention and directly illustrates that ATP synthesis per mole of cytochrome A is augmented by Ca^{2+} (Fig. 3). When combined, these data demonstrate that the activity of ANT and/or F_0/F_1-ATPase increased with [Ca^{2+}].

To further evaluate the rate limitations associated with ANT, F_0/F_1-ATPase, and cytochrome flux, the effects of the uncoupler FCCP were evaluated. FCCP, a proton ionophore, collapses the electrochemical gradient across the inner mitochondrial membrane, effec-

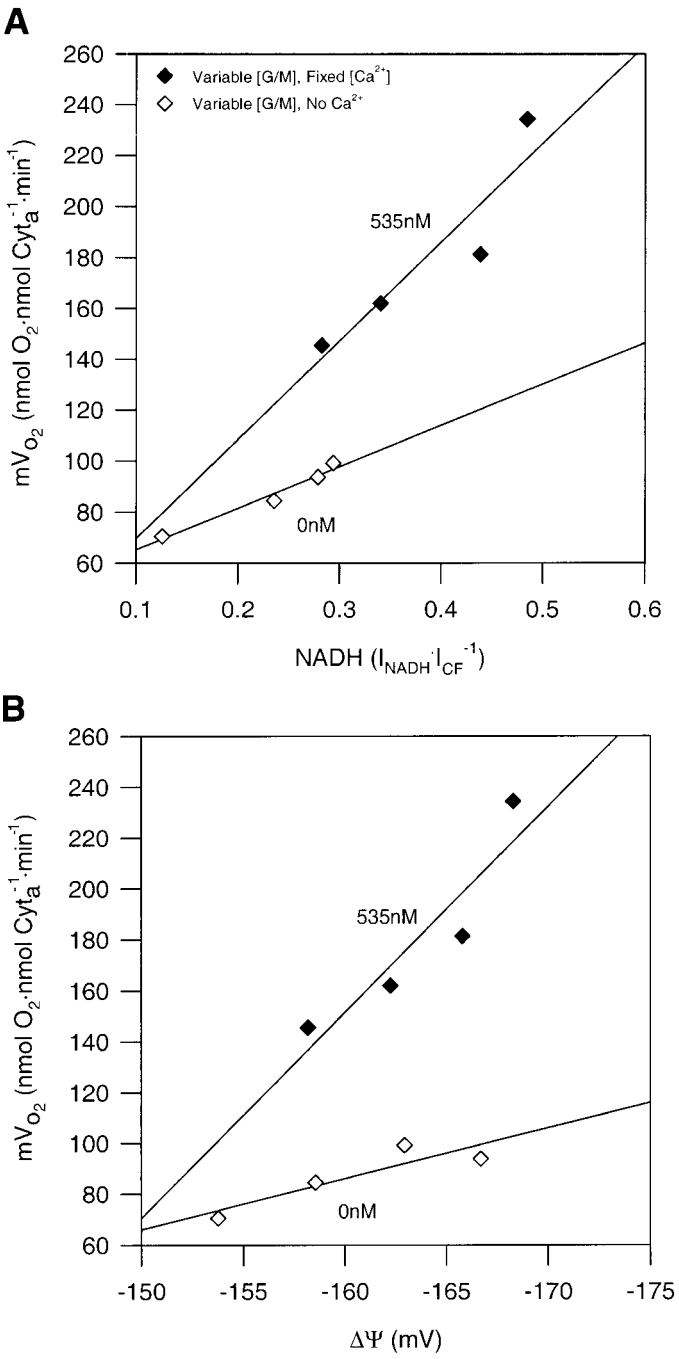

Fig. 5. Representative F-F relationships at state 3 respiration with variable substrates in presence and absence of Ca^{2+}. *A*: data are plotted as $m\dot{V}O_2$ vs. NADH, with filled symbols representing fixed [Ca^{2+}] (535 nM) and variable substrate concentrations, whereas open symbols are variable substrate concentrations minus additional Ca^{2+}. *B*: plot of $m\dot{V}O_2$ vs. $\Delta\psi$ in mitochondria oxidizing G/M (0.5–5 mM). In all cases, mitochondria were incubated at 37°C for 6 min, as described in MATERIALS AND METHODS, to Ca^{2+} deplete before commencement of experiments. Statistical analyses and degree of fit are presented in Table 3.

tively short-circuiting ANT and F_0/F_1-ATPase (3, 47). Under these conditions, it has been shown that $m\dot{V}O_2$ is dominated by the rate of NADH or $FADH_2$ formation and subsequent cytochrome oxidation. Thus FCCP effectively removes any rate limitation of ANT and

Table 4. *ADP/O ratios with substrate and Ca^{2+} titration*

[G/M], mM	[Ca^{2+}], nM	ADP/O	*n*
5/5	535	2.72 ± 0.03	8
2.5/2.5	535	2.75 ± 0.10	8
1.25/1.25	535	2.68 ± 0.07	9
0.63/0.63	535	2.67 ± 0.02	5
5/5	535	2.76 ± 0.08	10
5/5	167	2.76 ± 0.07	7
5/5	68	2.89 ± 0.15	4
5/5	31	2.73 ± 0.08	5
5/5	0	2.71 ± 0.07	9

Values are means ± SE. Substrate values are presented as equal proportions of glutamate (G) and malate (M). Free Ca^{2+} values were determined from published dissociation constants (23).

F_0/F_1-ATPase on $m\dot{V}O_2$. If Ca^{2+} stimulates $m\dot{V}O_2$ through ANT and/or F_0/F_1-ATPase, then the difference between FCCP-uncoupled and ADP-P_i-driven respiration should decrease as the inhibition of these enzymes is relieved with increasing [Ca^{2+}]. With the use of succinate to minimize the influence of CaDH, the percent difference between FCCP and maximal ADP-P_i-stimulated respiration was compared as a function of [Ca^{2+}] (Fig. 6). The percent difference between Ca^{2+}-stimulated and FCCP-uncoupled respiration decreased with increasing [Ca^{2+}], consistent with the notion that ANT and/or F_0/F_1-ATPase are activated by Ca^{2+}.

The effects of Ca^{2+} on the uncoupled rate of respiration yielded some insight into the Ca^{2+} effects and cytochrome flux. We estimated, using succinate, that only 10% of the Ca^{2+} stimulation of respiration was due to residual CaDH activation and was based on the increases in NADH observed with varying [Ca^{2+}] compared with the NADH standard curve (Fig. 4). Thus any adverse effects of Ca^{2+} on the uncoupled rate with

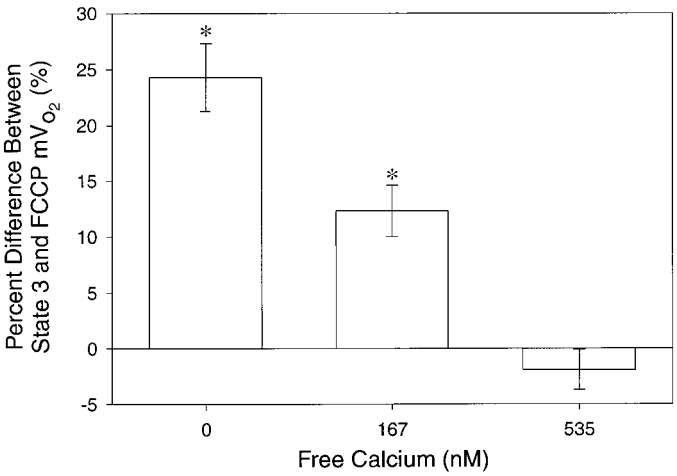

Fig. 6. Comparison of uncoupled and Ca^{2+}-stimulated coupled respiration. Plot of percentage difference between state 3 and FCCP-uncoupled respiration with increasing [Ca^{2+}]. State 3 respiration, oxidizing SUC (15 mM), was initiated with ADP (500 μM) after Ca^{2+} depletion. Maximally uncoupled respiration was achieved by titration of [FCCP] (33.3 nM final). Percent increase in $m\dot{V}O_2$ with uncoupler is plotted vs. free [Ca^{2+}]. Buffers and Ca^{2+} depletion were as indicated in Fig. 1. Data are means ± SE; *significant differences from state 3 ($P \leq 0.05$).

succinate should be due to cytochrome flux effects, such as direct activation of cytochrome oxidase (39). Uncoupled respiration increased by 10% with [Ca^{2+}]; however, these changes could be fully attributed to the small CaDH activation observed with succinate oxidation. Thus no evidence for Ca^{2+} stimulation of cytochrome activity was observed.

Interestingly, at the highest [Ca^{2+}] tested, the difference between uncoupled and ADP-P_i-driven respiration was not significantly different ($P \geq 0.05$, $n = 7$). For this to occur, all rate limitations upstream (i.e., dehydrogenases and cytochromes) would have to be negligible. These latter data suggest that a minimal limitation to ATP production rate exists at the level of ANT and/or F_0/F_1-ATPase when optimally activated by Ca^{2+}.

The effect of Ca^{2+} on oxidative phosphorylation observed could be due to direct activation of either ANT or F_0/F_1-ATPase as discussed above; however, the difficulty in isolating the effects of Ca^{2+} on intact mitochondrial ANT or F_0/F_1-ATPase is due to the close coupling of these enzyme complexes in the synthesis of ATP. To resolve this difficulty, arsenate (AsO_4) was used as a substrate for F_0/F_1-ATPase to remove the influence of ANT. In the absence of exogenous phosphate (P_i), AsO_4 uncouples ATP production from adenylate translocation, after initial loading with ADP, by synthesizing a metastable complex of ADP and AsO_4 within the matrix via the F_0/F_1-ATPase. The resulting ADP-AsO_4 complex undergoes rapid hydrolysis to re-form ADP and AsO_4, where the cycle is repeated (12, 26, 52, 68) (Fig. 7*A*). Oligomycin inhibits uncoupling by AsO_4; however, oligomycin does not prevent uncoupling by dinitrophenol (DNP) (22), therefore illustrating F_0/F_1-ATPase dependence of this agent. In all cases, mitochondria were preloaded with ADP (200 μM), where atractyloside (8.34 μM) was added to eliminate ANT contributions to the reaction. CaDH activation was minimized using succinate as the carbon substrate. Ca^{2+} stimulation of F_0/F_1-ATPase could be assessed directly using these conditions.

Addition of AsO_4 (2 mM) stimulated respiration by 2.4 ± 0.19-fold over the state 4 rate ($P \leq 0.05$, $n = 7$) and was totally inhibited with the addition of excess oligomycin B (310 μM), a specific inhibitor of the F_0/F_1-ATPase (Fig. 7*B*). These results are consistent with AsO_4 stimulating the F_0/F_1-ATPase directly as outlined above. The effects of [Ca^{2+}] on AsO_4-stimulated respiration are shown in Fig. 8. Ca^{2+} increased AsO_4-stimulated respiration above the CaDH effects on NADH or $\Delta\psi$ driving force and resulted in a greater than twofold higher NADH F-F slope in mitochondria oxidizing succinate as the carbon source (Fig. 8*A*; Table 3). Consistent with the effects of Ca^{2+} on ADP-P_i-driven respiration, the $\Delta\psi$ F-F function in AsO_4-stimulated mitochondria resulted in a decrease in $\Delta\psi$ and a reversal of $\Delta\psi$ F-F slope, with increasing [Ca^{2+}] (Fig. 8*B*; Table 3), and is consistent with direct activation of the F_0/F_1-ATPase. These results provide evidence that Ca^{2+} directly increases F_0/F_1-ATPase activity independent of CaDH- and ANT-mediated mechanisms.

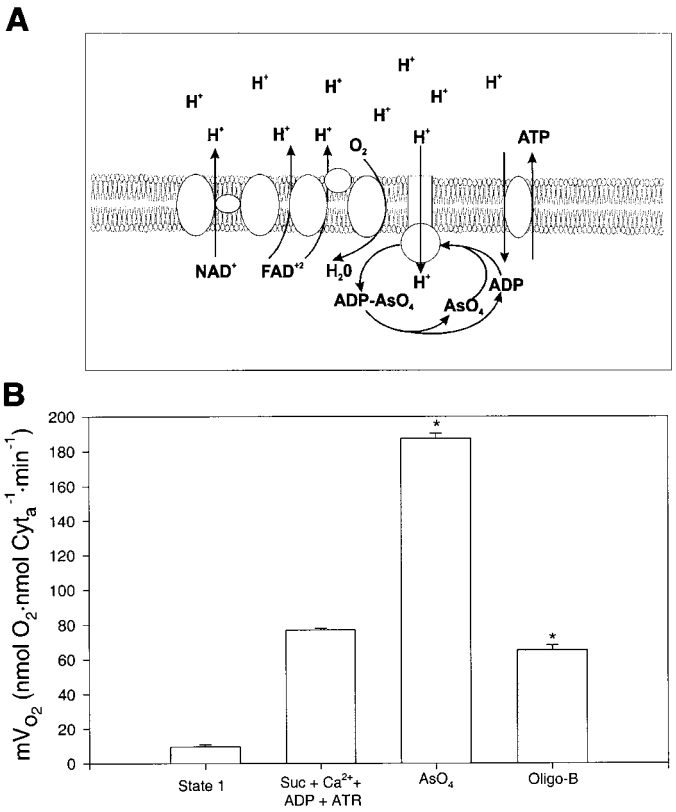

Fig. 7. *A*: schematic diagram of AsO_4-stimulated respiration. AsO_4-stimulated respiration is as described in text and was performed in presence of sufficient atractyloside to inhibit adenylate transport function (not shown) postloading with ADP. All other experimental protocols were performed as described in Fig. 4 legend with SUC as oxidizable carbon source. *B*: plot of $m\dot{V}_{O_2}$ with serial additions of substrates and metabolic inhibitors. Respiration was stimulated with 2 mM AsO_4 addition, after serially preloading with 200 μM ADP and 8.34 μM atractyloside, and was inhibited with excess oligomycin B (oligo B; 310 μM), illustrating F_0/F_1-ATPase dependence. Data are means ± SE; *significant differences from state 2 ($P \leq 0.05$).

DISCUSSION

Ca^{2+} activation of oxidative phosphorylation. Collectively, the current study suggests that Ca^{2+} enhanced ADP-P_i-driven respiration in heart mitochondria, and is not limited to CaDH activation alone. These data also suggest that a significant fraction of the matrix Ca^{2+}-stimulated ATP production is caused by direct activation of the F_0/F_1-ATPase with minimal metabolic uncoupling. With the use of the standard and experimental data with zero and optimal free [Ca^{2+}] (535 nM) at the same NADH driving force (i.e., 0.4 I_{NADH}/I_{CF}), it was calculated that the fraction of Ca^{2+}-stimulated ATP production by non-CaDH mechanisms was >60% (Fig. 4*A*).

The effects of Ca^{2+} on the CaDH have been well characterized in the literature (32, 48); however, evidence demonstrating direct Ca^{2+} stimulation of the F_0/F_1-ATPase and its mechanism to date is less clear (reviewed by Ref. 34). Several indirect studies from in situ cardiac biopsies (63), sonicated cardiomyocytes (14–17), and submitochondrial particles (62, 77) have implicated Ca^{2+} in the activation of F_0/F_1-ATPase; however, in most cases, ATP synthesis rates were

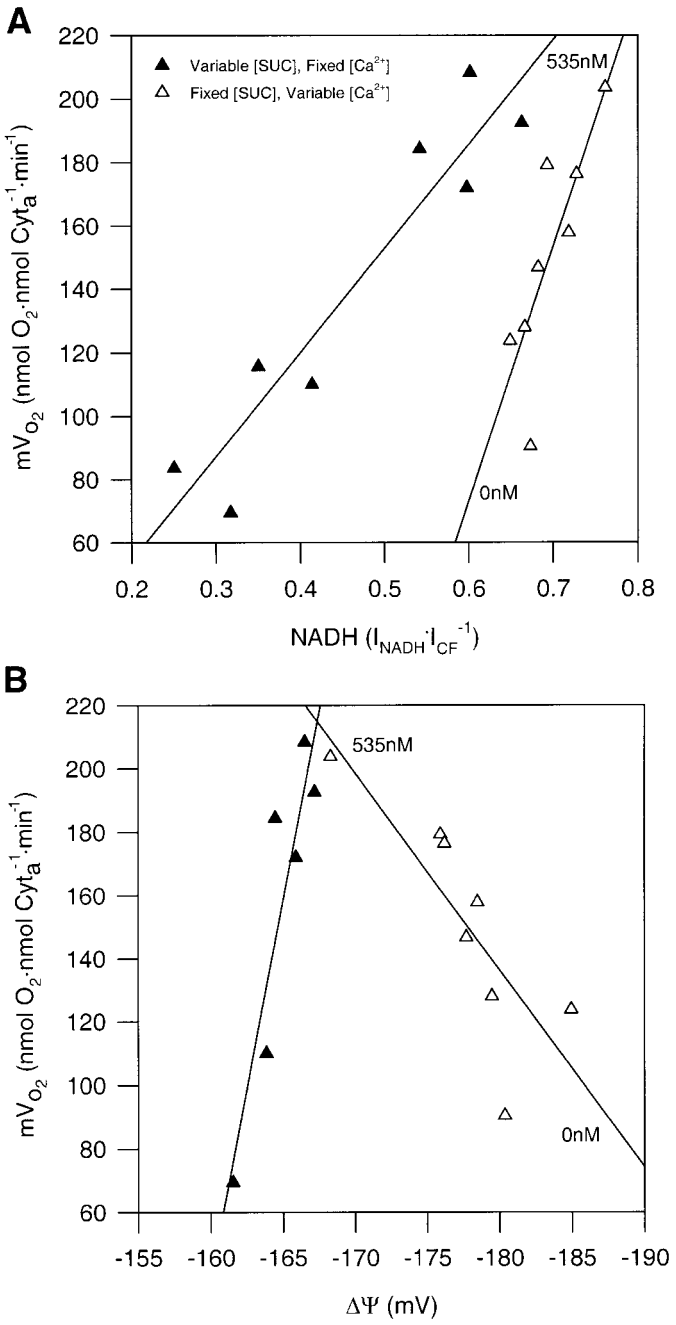

Fig. 8. Typical state 3 activation plot of F_0/F_1-ATPase by Ca^{2+}. *A*: data are plotted as $m\dot{V}O_2$ vs. NADH. In all cases, mitochondria were Ca^{2+} depleted, where 200 μM ADP and 8.34 μM atractyloside were added serially. Respiration was driven with a single addition of 2 mM AsO_4. Filled symbols represent fixed [Ca^{2+}] with variable [SUC] (control), whereas open symbols are mitochondria with variable [Ca^{2+}] with fixed [SUC]. *B*: plot of state 3 $m\dot{V}O_2$ and Δψ. All other conditions are as stated in Fig. 4*A* with SUC as oxidizable carbon source. Statistical analysis and results are presented in Table 3.

estimated from ATP hydrolysis rates in the absence of Δψ, a known regulator of oxidative phosphorylation (see Ref. 34). The meaning of these studies is, therefore, difficult to evaluate because the sites for hydrolysis and synthesis and their mechanisms are known to be distinct (see Ref. 4). Ca^{2+} is also known to bind to a number of matrix proteins, which include the Ca^{2+}-binding protein (CaBI) (75–77), cyclophilin D (11), and calmodulin (55), which in turn are known to alter membrane transport (11, 74) and/or ATP hydrolysis (77). Although these protein complexes interact with matrix Ca^{2+}, it is unclear how these translate to metabolic changes in heart mitochondria. Interestingly, matrix accumulation of Ca^{2+} has been shown to change the volume of heart mitochondria (25), which in turn is speculated to modify matrix enzyme activity (31) and, potentially, the F_0/F_1-ATPase. Any of the protein-binding modifications or volume changes could be responsible for the Ca^{2+} effects observed in this study.

Another mechanism for F_0/F_1-ATPase activation by Ca^{2+} would involve changes in the apparent K_m. Because the current experiments were conducted at saturating levels of substrates and ADP-P_i, it is therefore probable that Ca^{2+} activation involves an increase in the maximum velocity of F_0/F_1-ATPase or number of active enzyme complexes. As for direct effects on the F_0/F_1-ATPase, current theory holds that the major rate-limiting step in ATP formation is the release of ATP from the β-subunit (4). Therefore, if Ca^{2+} were acting directly on F_0/F_1-ATPase, it would likely lower the free energy for ATP release. To date, no evidence exists for direct interaction of Ca^{2+} with the F_0/F_1-ATPase; thus further studies are required to establish the exact mechanism of matrix Ca^{2+} actions.

In the current study, the net effect of Ca^{2+} was an increase in NADH levels and a decrease in Δψ at state 3. These data suggest that NAD^+/NADH and Δψ are not in equilibrium under these conditions because the net free energy for these intermediates moved in opposite directions with Ca^{2+} additions (Fig. 4). This suggests that a restriction in energy transfer exists between NADH and Δψ at site 1. The site of this restriction is unknown; however, similar results were found in working rat hearts (67), where increases in cardiac work and predictably higher mean cytosolic [Ca^{2+}] (6, 24) caused a fall in Δψ with increasing NADH. Therefore, the concordance of the data from intact mitochondria, cells, and hearts suggests that these isolated mitochondrial results may be applicable to the heart in vivo.

Despite the similarities with whole heart data, the question remains, are changes in the $[Ca^{2+}]_c$ with workload adequate to modify mitochondrial metabolism? Classical models suggest that mitochondrial Ca^{2+} uptake is too slow to match cytosolic Ca^{2+} transients during muscle contraction (69) and would instead track time-averaged $[Ca^{2+}]_c$. Indo 1 fluorescence studies in cardiac myocytes with Mn^{2+} quenching of Ca^{2+} signals seem to support this contention (50); however, these findings are complicated by accumulation and quenching by matrix Mn^{2+} (28). On the contrary, others have reported rapid mitochondrial Ca^{2+} uptake mechanisms (28, 64) and Ca^{2+} transients that track single myocyte contraction (7, 38, 66). Further support comes from work in isolated hepatocytes, where inositol trisphosphate-induced cytosolic Ca^{2+} waves are known to propagate into individual mitochondria (30), thus inducing a self-propagated intramitochondrial wave along the re-

ticular network (37). Irrespective of the mechanism and time course, Ca^{2+} is sequestered by mitochondria (29) when exposed to free $[Ca^{2+}]_c$ ranging from 100 to 1,200 nM (69, 71). Integrating these literature data over the cardiac cycle revealed a cytosolic time-averaged and end-diastolic concentrations of 345 and 115 nM, respectively. These findings are consistent with direct measures of mean free $[Ca^{2+}]_c$ in adult hamster myocytes at rest (200–300 nM) and with positive inotropic work (~400 nM) using indo 1/AM (6). Based on the integration and direct measurement data described above, it would appear that the $K_{0.5}$ for Ca^{2+} activation in this preparation (Table 1) is well within mean physiological levels and is even suited to achieve a reasonable dynamic range if beat-to-beat variations in matrix $[Ca^{2+}]$ occur. Of some importance may be the recent work on HeLa cells that demonstrated a close coupling between mitochondria and endo(sarco)plasmic reticulum (SR) $[Ca^{2+}]$ (58), which could result in microdomains of high $[Ca^{2+}]_c$ (57) in close proximity to the L-type Ca^{2+} channels. These latter results suggest a direct coupling of the SR and mitochondria bypassing the cytosolic pool altogether. This mechanism might permit a rapid transfer of Ca^{2+} to the mitochondrial matrix during contraction not available from classical isolated mitochondrial preparations.

There are several limitations to this study on Ca^{2+} effects on isolated mitochondria. First, any study on isolated mitochondria could suffer from isolation damage due to tissue preparation. Based on our RCR data, isolation damage was minimized because the coupling characteristics of this preparation were excellent (RCR $\cong$ 10), and high ATP production rates per cytochrome A in this preparation were achieved. However, these measures provide only limited information in a very complex process. Second, the depletion of Ca^{2+} is problematic because it is unclear what the resting matrix $[Ca^{2+}]$ is in vivo. Therefore, it is difficult to know whether our protocol mimics the intact heart appropriately. Finally, Ca^{2+} transport can uncouple and overload mitochondria, resulting in significant membrane permeability changes or damage (46). As such, care was taken to select a $[Ca^{2+}]$ within the physiological range that would not have significant pathophysiological or uncoupling effects. This was evaluated using two separate estimates of the ADP/O ratio, and, in both cases, no evidence for significant uncoupling was observed. Therefore, at 535 nM $[Ca^{2+}]$, coupling and reducing equivalent flow from reducing equivalents to ATP production in this preparation were maintained.

In summary, these observations suggest that increased systolic Ca^{2+} and subsequent stimulation of myocardial work at the actin-myosin ATPase could be paralleled by an activation of mitochondrial ATP production at several levels. It is interesting to note that, as in the cytosol where Ca^{2+} increases work and biochemical energy conversion in concert, the present data suggest a similar mode of operation within the mitochondria itself; i.e., Ca^{2+} increases the driving force through CaDH as well as activates the ATP production steps (i.e., work) directly. This form of parallel stimulation in a physiological control network provides a mechanism of increasing flux with minimal perturbations on the potentially important intermediates of the reactions. Finding this type of regulation on two levels of bioenergetics in the heart, the cytosol, and within the mitochondria by Ca^{2+} may suggest that this is an important general mechanism in cellular metabolic regulation.

Present address of V. K. Mootha: Dept. of Medicine, Brigham and Women's Hospital, 75 Francis St., Boston, MA 02115.

Address for reprint requests and other correspondence: P. R. Territo, Laboratory of Cardiac Energetics, National Heart, Lung, and Blood Institute, National Institutes of Health, Bldg. 10, Rm. B1D-416, Bethesda, MD 20892-1061 (E-mail: territop@zeus.nhlbi.nih.gov).

Received 20 January 1999; accepted in final form 14 September 1999.

REFERENCES

1. **Balaban, R. S., H. L. Kantor, L. A. Katz, and R. W. Briggs.** Relation between work and phosphate metabolite in the in vivo paced mammalian heart. *Science* 232: 1121–1123, 1986.
2. **Balaban, R. S., V. K. Mootha, and A. Arai.** Spectroscopic determination of cytochrome c oxidase content in tissues containing myoglobin or hemoglobin. *Anal. Biochem.* 237: 274–278, 1996.
3. **Benz, R., and S. McLaughlin.** The molecular mechanism of action of the proton ionophore FCCP (carbonyl cyanide *p*-trifluoromethoxyphenylhydrazone). *Biophys. J.* 41: 381–398, 1983.
4. **Boyer, P. D.** The ATP synthase–a splendid molecular machine. *Annu. Rev. Biochem.* 66: 717–749, 1997.
5. **Bunger, R., and B. Permanetter.** Parallel stimulation by Ca^{2+} of inotropism and pyruvate dehydrogenase in perfused heart. *Am. J. Physiol. Cell Physiol.* 247: C45–C52, 1984.
6. **Buser, P. T., S. Y. Wu, W. W. Parmley, G. Jasmin, and J. Wikman-Coffelt.** Distinct modulation of myocardial performance, energy metabolism, and $[Ca^{2+}]$i transients by positive inotropic drugs in normal and severely failing hamster hearts. *Cardiovasc. Drugs Ther.* 9: 151–157, 1995.
7. **Chacon, E., H. Ohata, I. S. Harper, D. R. Trollinger, B. Herman, and J. J. Lemasters.** Mitochondrial free Ca^{2+} transients during excitation-contraction coupling in rabbit cardiac myocytes. *FEBS Lett.* 382: 31–36, 1996.
8. **Chance, B., and G. Williams.** Respiratory enzymes in oxidative phosphorylation: I. Kinetics of oxygen utilization. *J. Biol. Chem.* 217: 383–393, 1955.
9. **Chappell, J.** The oxidation of citrate, isocitrate, and *cis*-aconitate by isolated mitochondria. *Biochem. J.* 90: 225–237, 1964.
10. **Cohen, S. S.** Are/were mitochondria and chloroplasts microorganisms? *Am. Sci.* 58: 281–289, 1970.
11. **Connern, C. P., and A. P. Halestrap.** Chaotropic agents and increased matrix volume enhance binding of mitochondrial cyclophilin to the inner mitochondrial membrane and sensitize the mitochondrial permeability transition to $[Ca^{2+}]$. *Biochemistry* 35: 8172–8180, 1996.
12. **Crane, R., and F. Lipman.** The effects of arsenate on aerobic phosphorylation. *J. Biol. Chem.* 201: 235–243, 1953.
13. **Crompton, M., and I. Heid.** The cycling of Ca^{2+}, sodium, and protons across the inner membrane of cardiac mitochondria. *Eur. J. Biochem.* 91: 599–608, 1978.
14. **Das, A. M., and D. A. Harris.** Control of mitochondrial ATP synthase in heart cells: inactive to active transitions caused by beating or positive inotropic agents. *Cardiovasc. Res.* 24: 411–417, 1990.
15. **Das, A. M., and D. A. Harris.** Control of mitochondrial ATP synthase in rat cardiomyocytes: effects of thyroid hormone. *Biochim. Biophys. Acta* 1096: 284–290, 1991.
16. **Das, A. M., and D. A. Harris.** Intracellular Ca^{2+} as a regulator of the mitochondrial ATP synthase in cultured cardiomyocytes. *Biochem. Soc. Trans.* 18: 554–555, 1990.
17. **Das, A. M., and D. A. Harris.** Reversible modulation of the mitochondrial ATP synthase with energy demand in cultured rat cardiomyocytes. *FEBS Lett.* 256: 97–100, 1989.

18. **DeLuca, M., and W. D. McElroy.** Kinetics of the firefly luciferase catalyzed reactions. *Biochemistry* 13: 921–925, 1974.
19. **DeLuca, M., J. Wannlund, and W. D. McElroy.** Factors affecting the kinetics of light emission from crude and purified firefly luciferase. *Anal. Biochem*. 95: 194–198, 1979.
20. **Detre, J. A., D. S. Williams, and A. P. Koretsky.** Nuclear magnetic resonance determination of flow, lactate, and phosphate metabolites during amphetamine stimulation of the rat brain. *NMR Biomed*. 3: 272–278, 1990.
21. **Doeller, J. E., and B. A. Wittenberg.** Intracellular Ca^{2+} and high-energy phosphates in isolated cardiac myocytes. *Am. J. Physiol. Heart Circ. Physiol.* 259: H1851–H1859, 1990.
22. **Estabrook, R.** Effects of oligomycine on the arsenate and DNP stimulation of mitochondrial oxidation. *Biophys. Biochem. Res. Com*. 4: 89–91, 1961.
23. **Fabiato, A., and F. Fabiato.** Calculator programs for computing the composition of the solutions containing multiple metals and ligands used for experiments in skinned muscle cells. *J. Physiol. Paris* 75: 463–505, 1979.
24. **Fralix, T. A., F. W. Heineman, and R. S. Balaban.** Effect of work on intracellular Ca^{2+} of the intact heart. *Am. J. Physiol.* Suppl. (Oct.) 261: 78–80, 1991.
25. **French, S. A., P. R. Territo, and R. S. Balaban.** Correction for inner filter effects in turbid samples: fluorescence assays of mitochondrial NADH. *Am. J. Physiol. Cell Physiol.* 275: C900–C909, 1998.
26. **Gresser, M. J.** ADP-arsenate. Formation by submitochondrial particles under phosphorylating conditions. *J. Biol. Chem*. 256: 5981–5983, 1981.
27. **Gunter, T. E.** Cation transport by mitochondria. *J. Bioenerg. Biomembr.* 26: 465–469, 1994.
28. **Gunter, T. E., L. Buntinas, G. C. Sparagna, and K. K. Gunter.** The Ca^{2+} transport mechanisms of mitochondria and Ca^{2+} uptake from physiological-type Ca^{2+} transients. *Biochim. Biophys. Acta* 1366: 5–15, 1998.
29. **Gunter, T. E., K. K. Gunter, S. S. Sheu, and C. E. Gavin.** Mitochondrial Ca^{2+} transport: physiological and pathological relevance. *Am. J. Physiol. Cell Physiol.* 267: C313–C339, 1994.
30. **Hajnoczky, G., L. D. Robb-Gaspers, M. B. Seitz, and A. P. Thomas.** Decoding of cytosolic calcium oscillations in the mitochondria. *Cell* 82: 415–424, 1995.
31. **Halestrap, A. P.** The regulation of the matrix volume of mammalian mitochondria in vivo and in vitro and its role in the control of mitochondrial metabolism. *Biochim. Biophys. Acta* 973: 355–382, 1989.
32. **Hansford, R. G., R. Moreno-Sanchez, and B. Lewartowski.** Activation of pyruvate dehydrogenase complex by Ca^{2+} in intact heart, cardiac myocytes, and cardiac mitochondria. *Ann. NY Acad. Sci.* 573: 240–253, 1989.
33. **Hansford, R. G., and D. Zorov.** Role of mitochondrial calcium transport in the control of substrate oxidation. *Mol. Cell. Biochem*. 184: 359–369, 1998.
34. **Harris, D. A., and A. M. Das.** Control of mitochondrial ATP synthesis in the heart. *Biochem. J.* 280: 561–573, 1991.
35. **Heineman, F. W., and R. S. Balaban.** Effects of afterload and heart rate on NAD(P)H redox state in the isolated rabbit heart. *Am. J. Physiol. Heart Circ. Physiol.* 264: H433–H440, 1993.
36. **Hinkle, P. C., and M. L. Yu.** The phosphorus/oxygen ratio of mitochondrial oxidative phosphorylation. *J. Biol. Chem*. 254: 2450–2455, 1979.
37. **Ichas, F., L. S. Jouaville, and J. P. Mazat.** Mitochondria are excitable organelles capable of generating and conveying electrical and calcium signals. *Cell* 89: 1145–1153, 1997.
38. **Isenberg, G., S. Han, A. Schiefer, and M. F. Wendt-Gallitelli.** Changes in mitochondrial calcium concentration during the cardiac contraction cycle. *Cardiovasc. Res.* 27: 1800–1809, 1993.
39. **Kadenbach, B., and S. Arnold.** A second mechanism of respiratory control. *FEBS Lett.* 447: 131–134, 1999.
40. **Katz, L. A., J. A. Swain, M. A. Portman, and R. S. Balaban.** Relation between phosphate metabolites and oxygen consumption of heart in vivo. *Am. J. Physiol. Heart Circ. Physiol.* 256: H265–H274, 1989.
41. **Koretsky, A. P.** Insights into cellular energy metabolism from transgenic mice. *Physiol. Rev.* 75: 667–688, 1995.
42. **Koretsky, A. P., and R. S. Balaban.** Changes in pyridine nucleotide levels alter oxygen consumption and extra-mitochondrial phosphates in isolated mitochondria: a 31P-NMR and NAD(P)H fluorescence study. *Biochim. Biophys. Acta* 893: 398–408, 1987.
43. **Koretsky, A. P., L. A. Katz, and R. S. Balaban.** The mechanism of respiratory control in the in vivo heart. *J. Mol. Cell. Cardiol.* 21, *Suppl.* 1: 59–66, 1989.
44. **Lemasters, J. J., and C. E. Hackenbrock.** Adenosine triphosphate: continuous measurement in mitochondrial suspension by firefly luciferase luminescence. *Biochem. Biophys. Res. Commun.* 55: 1262–1270, 1973.
45. **Lemasters, J. J., and C. R. Hackenbrock.** Continuous measurement of adenosine triphosphate with firefly luciferase luminescence. *Methods Enzymol.* 56: 530–544, 1979.
46. **Lemasters, J. J., A. L. Nieminen, T. Qian, L. C. Trost, S. P. Elmore, Y. Nishimura, R. A. Crowe, W. E. Cascio, C. A. Bradham, D. A. Brenner, and B. Herman.** The mitochondrial permeability transition in cell death: a common mechanism in necrosis, apoptosis and autophagy. *Biochim. Biophys. Acta* 1366: 177–196, 1998.
47. **Matsuno-Yagi, A., and Y. Hatefi.** Uncoupling of oxidative phosphorylation: different effects of lipophilic weak acids and electrogenic ionophores on the kinetics of ATP synthesis. *Biochemistry* 28: 4367–4374, 1989.
48. **McCormack, J. G., and R. M. Denton.** The role of mitochondrial Ca^{2+} transport and matrix Ca^{2+} in signal transduction in mammalian tissues. *Biochim. Biophys. Acta* 1018: 287–291, 1990.
49. **McCormack, J. G., A. P. Halestrap, and R. M. Denton.** Role of calcium ions in regulation of mammalian intramitochondrial metabolism. *Physiol. Rev.* 70: 391–425, 1990.
50. **Miyata, H., H. S. Silverman, S. J. Sollott, E. G. Lakatta, M. D. Stern, and R. G. Hansford.** Measurement of mitochondrial free Ca^{2+} concentration in living single rat cardiac myocytes. *Am. J. Physiol. Heart Circ. Physiol.* 261: H1123–H1134, 1991.
51. **Mootha, V. K., A. E. Arai, and R. S. Balaban.** Maximum oxidative phosphorylation capacity of the mammalian heart. *Am. J. Physiol. Heart Circ. Physiol.* 272: H769–H775, 1997.
52. **Moreno-Sanchez, R.** Contribution of the translocator of adenine nucleotides and the ATP synthase to the control of oxidative phosphorylation and arsenylation in liver mitochondria. *J. Biol. Chem*. 260: 12554–12560, 1985.
53. **Moreno-Sanchez, R., and R. G. Hansford.** Dependence of cardiac mitochondrial pyruvate dehydrogenase activity on intramitochondrial free Ca^{2+} concentration. *Biochem. J.* 256: 403–412, 1988.
54. **Moreno-Sanchez, R., B. A. Hogue, and R. G. Hansford.** Influence of NAD-linked dehydrogenase activity on flux through oxidative phosphorylation. *Biochem. J.* 268: 421–428, 1990.
55. **Pedersen, P. L., and J. Hullihen.** Inhibitor peptide of mitochondrial proton adenosine triphosphatase. Neutralization of its inhibitory action by calmodulin. *J. Biol. Chem*. 259: 15148–15153, 1984.
56. **Rios, E., and M. D. Stern.** Calcium in close quarters: microdomain feedback in excitation-contraction coupling and other cell biological phenomena. *Annu. Rev. Biophys. Biomol. Struct.* 26: 47–82, 1997.
57. **Rizzuto, R., M. Brini, M. Murgia, and T. Pozzan.** Microdomains with high Ca^{2+} close to IP3-sensitive channels that are sensed by neighboring mitochondria. *Science* 262: 744–747, 1993.
58. **Rizzuto, R., P. Pinton, W. Carrington, F. S. Fay, K. E. Fogarty, L. M. Lifshitz, R. A. Tuft, and T. Pozzan.** Close contacts with the endoplasmic reticulum as determinants of mitochondrial Ca^{2+} responses. *Science* 280: 1763–1766, 1998.
59. **Rottenberg, H.** Membrane potential and surface potential in mitochondria: uptake and binding of lipophilic cations. *J. Membr. Biol.* 81: 127–138, 1984.
60. **Rottenberg, H.** The thermodynamic description of enzyme-catalyzed reactions. The linear relation between the reaction rate and the affinity. *Biophys. J.* 13: 503–511, 1973.

61. **Rottenberg, H., and A. Scarpa.** Calcium uptake and membrane potential in mitochondria. *Biochemistry* 13: 4811–4817, 1974.
62. **Rouslin, W., and C. W. Broge.** Factors affecting the reactivation of the mitochondrial adenosine 5′-triphosphatase and the release of ATPase inhibitor protein during and following the reenergization of mitochondria from ischemic cardiac muscle. *Arch. Biochem. Biophys.* 275: 385–394, 1989.
63. **Scholz, T. D., and R. S. Balaban.** Mitochondrial F1-ATPase activity of canine myocardium: effects of hypoxia and stimulation. *Am. J. Physiol. Heart Circ. Physiol.* 266: H2396–H2403, 1994.
64. **Sparagna, G. C., K. K. Gunter, S. S. Sheu, and T. E. Gunter.** Mitochondrial calcium uptake from physiological-type pulses of calcium. A description of the rapid uptake mode. *J. Biol. Chem.* 270: 27510–27515, 1995.
65. **Stucki, J. W., M. Compiani, and S. R. Caplan.** Efficiency of energy conversion in model biological pumps. Optimization by linear nonequilibrium thermodynamic relations. *Biophys. Chem.* 18: 101–109, 1983.
66. **Trollinger, D. R., W. E. Cascio, and J. J. Lemasters.** Selective loading of Rhod 2 into mitochondria shows mitochondrial Ca^{2+} transients during the contractile cycle in adult rabbit cardiac myocytes. *Biochem. Biophys. Res. Commun.* 236: 738–742, 1997.
67. **Wan, B., C. Doumen, J. Duszynski, G. Salama, T. C. Vary, and K. F. LaNoue.** Effects of cardiac work on electrical potential gradient across mitochondrial membrane in perfused rat hearts. *Am. J. Physiol. Heart Circ. Physiol.* 265: H453–H460, 1993.
68. **Welle, H. F., and E. C. Slater.** Uncoupling of respiratory-chain phosphorylation by arsenate. *Biochim. Biophys. Acta* 143: 1–17, 1967.
69. **Wier, W.** $[Ca^{2+}]_i$ Transients during excitation-contraction coupling of mammalian heart. In: *The Heart and Cardiovascular System (2nd ed.)*, edited by H. Fozzard. New York: Raven, 1992, p. 1223–1248.
70. **Wier, W. G., J. R. Lopez-Lopez, P. S. Shacklock, and C. W. Balke.** Calcium signaling in cardiac muscle cells. *Ciba Found. Symp.* 188: 146–160.
71. **Wier, W. G., and D. T. Yue.** Intracellular calcium transients underlying the short-term force-interval relationship in ferret ventricular myocardium. *J. Physiol. (Lond.)* 376: 507–530, 1986.
72. **Wingard, C. J., R. J. Paul, and R. A. Murphy.** Energetic cost of activation processes during contraction of swine arterial smooth muscle. *J. Physiol. (Lond.)* 501: 213–223, 1997.
73. **Wolff, S. D., C. Eng, and R. S. Balaban.** NMR studies of renal phosphate metabolites in vivo: effects of hydration and dehydration. *Am. J. Physiol. Renal Fluid Electrolyte Physiol.* 255: F581–F589, 1988.
74. **Woodfield, K., A. Ruck, D. Brdiczka, and A. P. Halestrap.** Direct demonstration of a specific interaction between cyclophilin-D and the adenine nucleotide translocase confirms their role in the mitochondrial permeability transition. *Biochem. J.* 336: 287–290, 1998.
75. **Yamada, E. W., and N. J. Huzel.** Ca^{2+}-binding properties of a unique ATPase inhibitor protein isolated from mitochondria of bovine heart and rat skeletal muscle. *Cell Calcium* 6: 469–479, 1985.
76. **Yamada, E. W., and N. J. Huzel.** The calcium-binding ATPase inhibitor protein from bovine heart mitochondria. Purification and properties. *J. Biol. Chem.* 263: 11498–11503, 1988.
77. **Yamada, E. W., and N. J. Huzel.** Calcium-binding ATPase inhibitor protein of bovine heart mitochondria. Role in ATP synthesis and effect of Ca^{2+}. *Biochemistry* 28: 9714–9718, 1989.